Integration of gene expression data in Bayesian association analysis of rare variants

Guojie Zhong[1,2], Yoolim A. Choi[3], Yufeng Shen[1,3,4]

1. Department of Systems Biology
2. Integrated Program in Cellular, Molecular, and Biomedical Studies
3. Department of Biomedical Informatics
4. JP Sulzberger Columbia Genome Center

Columbia University Irving Medical Center, New York, NY

Contact: Y.S., ys2411@cumc.columbia.edu

Abstract

We present two new methods, xTADA and VBASS (Variational inference Bayesian ASSociation), that integrate expression data to improve power of rare variants association analysis. Optimized for bulk RNA-seq and single-cell transcriptomics data respectively, xTADA and VBASS model the association of disease risk as a function of expression profiles of relevant tissue or cell types in Bayesian frameworks. On simulated data, both methods show proper error rate control and better power than extTADA, the state-of-the-art Bayesian method. We applied the methods to published datasets and identified more candidate risk genes than extTADA with supports from literature or data from independent cohorts.

Background

About 3% of children are born with congenital anomalies or will develop neurodevelopmental disorders (NDD)[1]. Given the severe consequence of these conditions on reproductive fitness, risk variants with large effect are under strong negative selection and therefore have low frequency in the population. Recent genetics studies identified hundreds of risk genes of these conditions, largely by rare *de novo* variants[2-11], however, the majority of risk genes remain unidentified[10,12-15], due to challenges in statistical power in analysis of rare variants[16].

Cell-type specific gene expression has long been used qualitatively for interpretation of biological mechanisms in developmental biology and genetics. Previously we have shown that high expression in developing heart and diaphragm is associated with increased burden of de novo coding variants in congenital heart disease (CHD)[7] and congenital diaphragmatic hernia[9], respectively. We have also shown that cell-type specific expression in brain is associated with plausibility of autism spectrum disorders (ASD) risk genes[17,18]. It is clear that gene expression profile can inform association analysis of rare variants for risk gene discovery. However, the ability to improve power in gene discovery using expression data has been hindered by the lack of rigorous statistical methods and cell type specific expression data from relevant tissues during development. Recent efforts in cell atlas of human and model organisms have been generating large amount of single cell expression data of adult tissues[19,20] in addition to an increase in various developmental stages[21-24]. Here we describe two computational methods that leverage expression data with probabilistic models to improve statistical power of risk gene discovery.

The first method, xTADA, has a similar structure as extTADA[12,25], an empirical Bayes method for association of *de novo* and rare variants. xTADA takes a single gene expression profile, such as bulk RNA-seq, as a separate observed variable independent of genetic variants conditioned on risk status. In xTADA, the expression level of a gene is a random variable that has different distributions under the null and the alternative models. Like TADA[12] and extTADA[25], it learns the priors of the model using the observed *de novo* variants in cases across genes without explicit knowledge of known risk genes. The second method, VBASS (Variational inference Bayesian ASSociation), takes a vector of expression profile, such as cell-type specific expression from single cell RNA-seq and models the priors of risk genes as a function of expression profile of multiple cell types. VBASS uses deep neural networks to approximate the function and uses semi-supervised variational inference to estimate the parameters. We compared the performances of both methods with extTADA by both simulated and published de novo variants datasets to assess error control and statistical power.

Results

Model architectures

x-TADA is a Bayesian mixture model that extends the TADA framework[12] by making expression data as an observation of a gene in addition to *de novo* variants data. It assumes that under the null (H_0), the ranked expression level follows a uniform distribution, and under the alternative (H_1), the rank follows a sigmoid function determined by 3 parameters (A, B, C) with more probability density in higher expression (Figure 1A, methods). We use this distribution to quantify the fact that genes with higher expression in the corresponding organ are more likely to harbor disease risk variants. Assuming expression data and de novo variant data are independently conditioned on H_0 and H_1, the likelihood term is calculated by mixture of joint distributions (Methods). We estimated all parameters in the model from whole gene set in an unbiased manner using MCMC via rstan package (Methods). The parameters were then used to calculate the posterior probability of association (PPA) for each gene to disease risk as well as the false discovery rate (FDR, Methods).

VBASS is a Bayesian mixture model with learnable priors through variational inference (Figure 1B). We model the number of genetic variants of interest (e.g., LGD or Dmis de novo variants) in the gene d_{gv} as a sample drawn independently through mixture of Poisson and Gamma-Poisson (Negative binomial) Distributions $p(d_{gv}|\gamma_{gv}, M_{gv}, y_g)$ conditioned on a binary random variable y_g that indicates whether the gene is a risk gene or not, background mutation rate M_{gv} and relative risk γ_{gv} (Methods). y_g follows a Bernoulli distribution with parameter π_g, which represents the gene specific prior of disease risk. We model this prior as a function of expression profiles x_g that could be inferred with a neural network f_E (Fig. 1B, Methods). γ_{gv} is a random variable that denotes the enrichment rate of damage variant v in the patient cohort, which is also known as the relative risk of this gene. γ_{gv} is drawn independently through Gamma distribution $p(\gamma_{gv}|k_{gv}, \theta_{gv})$. k_{gv}, θ_{gv} are conditioned on y_g, under null they are equal to 1 while under alternative, they are equal to $\overline{k_v}$ and $\overline{\theta_v}$, respectively. We assume $\overline{k_v}$ and $\overline{\theta_v}$ are shared across all disease risk genes (Methods). We trained VBASS in a semi-supervised manner and used estimated parameters to calculate PPA and FDR (Methods).

xTADA showed better power than extTADA on simulated data

We tested the performance of xTADA and extTADA on simulated CHD dataset (Method). As expected, both models showed good false discovery control and local false discovery control (Sup Fig. 1). xTADA outperformed extTADA with better recall under same precision level (Fig. 2A) under sample sizes from 2,645-20,000. Although the difference in power decreases with increasing sample size, xTADA still outperformed extTADA by roughly 10% increase of recall at sample size of 10,000, which is feasible for CHD in the next few years.

To test the power of xTADA with respect to the size of genes, we calculated the recall rate at same significance levels (FDR ≤ 0.05) on both models for genes with different mutation rates. xTADA showed better statistical power especially for genes with higher mutation rates under small sample sizes (Fig. 2B). As the sample size increases, the power difference of xTADA and extTADA becomes smaller on large genes, while xTADA still outperforms extTADA on medium-mutation-rate genes (Fig. 2B). Overall, our simulation results showed that xTADA can increase the statistical power for prioritizing disease risk genes by taking expression data as an additional covariate.

VBASS showed better power than extTADA on simulated data

We ran VBASS and extTADA separately on the simulation dataset (Method). Both models showed good false discovery control (Fig. 3A). To test the statistical power of VBASS and extTADA, we plotted the precision-recall curve using the output posterior probabilities from VBASS, extTADA and the real parameters we used in simulation. VBASS outperformed extTADA with higher recall under same precision (Fig. 3B). Further comparison showed good correlation between the prior value $\bar{\pi}_g$ informed by VBASS and real π_g we used in simulation (Fig. 3C), indicating that VBASS could reconstruct the prior of being risk through single cell expression data. Moreover, we assessed the association between expression profile x and π via spearman correlation, the result of VBASS is close to real values (Fig. 3D). Overall, those results showed that our model can not only reach higher statistical power on simulation data set than extTADA but also uncover the association between cell type expression profiles and disease risk.

xTADA identified novel CHD candidate risk genes on published DNV data

We applied xTADA to a CHD data set with DNVs from 2645 trios[13]. We used the mouse embryonic E14.5 heart bulk RNA-seq data to set gene expression rank percentile[6,7]. The estimated distribution of expression rank under null and alternative hypothesis showed most of the risk genes are enriched in rank percentile ≥ 75% (genes with rank percentile ≥ 0.75 are roughly 3 times more likely to be risk than other genes) (Fig. 4A, Table 1), consistent with previous burden analysis of de novo variants[7]. With FDR ≤ 0.1, we identified 49 candidate risk genes. In contrast, using the original TADA method, we were able to identify only 40 candidate genes (Fig. 4B, 4C, Table 2, Table S4). Among the gene that only detected by xTADA, *FLT4* was reported to be a risk gene via combined analysis of *de novo* and inherited variants in the original paper, while *TSC1* and *FBN1* were in their curated CHD gene dataset from literature search[13,26]. *CHD4* was reported to be significantly associated with CHD in a UK CHD cohort of 1891 probands[8], while 3 (*FRYL*, *SETD5*, *KMT2C*) have both LoF and missense variants carriers, 2 (*GANAB*, *KDM5A*) have only missense variants carriers in that cohort. Furthermore, 4 (*CHD4*, *SETD5*, *KMT2C*, *FBN1*) are significantly associated with neurodevelopmental disorders[27], while 11 (*CHD4*, *FRYL*, *GANAB*, *SETD5*, *MINK1*, *ANK3*, *KMT2C*, *IQGAP1*, *TSC1*, *KDM5A*, *FBN1*) have both LoF and missense variants carriers, and 2 (*CAD*, *SLIT3*) have only missense variants carriers in that cohort. Overall, these genes have additional genetic evidence in other cohorts and are plausible candidates. These results indicate that the assumption of xTADA is biologically sound and suggests its higher statistical power even in lower cohort size.

VBASS identified novel ASD candidate risk genes on published DNV data

Previous studies have shown that gene expression in multiple cell types in the brain is associated with ASD risk[17,18,28]. This is in part what motivated the design of VBASS. We obtained ASD DNV data from a recent preprint[15] that combined exome and genome data from four studies (see Methods), and single cell RNA-seq data of human fetal midbrain and prefrontal cortex from two publications[21,22]. We applied VBASS and extTADA to the full ASD data set with 16616 trios. VBASS identified 124 genes with PPA above 0.8 (Table S5). To compare the performance in identification of novel candidate risk genes, we removed the known risk genes used in training and calculate Bayesian FDR of all other genes with VBASS and extTADA (methods). Then we compared the candidate genes identified by VBASS and extTADA at significance level 0.05 and 0.1 (FDR ≤ 0.05 and FDR ≤ 0.1 respectively). At significance level 0.05, VBASS identified 51 genes (Table S6), among which 5 were not identified as candidates by extTADA (Fig. 5A, Table S6). Among the 5 genes, 2 (*DLG4, PAX5*) were reported to be risk genes in SFARI[29] data base (release 2021 Q4) with score of 1 while not in our training gene list. *METTL23* is a transcriptional partner of GABPA and essential for human recognition[30], and disruption of *METTL23* was reported to cause mild autosomal recessive intellectual disability[31]. *ATF4* was reported to have significant altered expression in the middle frontal gyrus of ASD subjects[32]. At significance level 0.1, VBASS identified 75 genes (Table S6), where 6 were not identified by extTADA (Fig. 5A, Table S6). Among the 6 genes, 2 (*ZMYND8 CASZ1*) were scored 1 in SFARI data base and *CMPK2* was scored 3. *LMTK3* was reported to cause behavioral abnormalities such as locomotor hyperactivity and reduced anxiety in mice knock-out models[33,34]. Furthermore, 7 out of the 11 genes identified only by VBASS (*DLG4, METTL23, SPRY2, LMTK3, PFN2, CASZ1, ZMYND8*) have additional genetic evidence in related cohorts[27]. There were six genes (*CCDC40, FUBP3, PRKAR1B, SIN3A, ITGB5, PMM2*) identified only by extTADA but not by VBASS, likely because of their low detection rates or co-expression strength with other candidates in the single cell datasets. Finally, we studied what are the cell types that associated the most with disease risk. According to spearman correlation analysis, we showed that oculomotor / trochlear nucleus (hOMTN), GABAergic neurons (hGaba) and dopaminergic neurons (hDA1) in gestation week 9-10 are more associated with autism risk, while microglia cells and endothelial cells (hEndo) are less associated with autism risk (Fig. 5C). This observation is consistent with previous evidence of abnormalities in GABAergic neurons and synapses in neurodevelopmental disorders characterized by a shared symptomatology of ASD symptoms[35], while reductions in GABA have been reported in several brain regions in children with ASD[36,37]. There were also evidences that dopaminergic dysfunctions were associate with autistic-like behavior[38,39].

Discussion and conclusions

In this study, we described two new methods, xTADA and VBASS, for identification of candidate risk genes by joint analysis of de novo variants of cases and gene expression profile of normal samples. The core idea of both methods is that prior probability of a gene increase disease risk is a function of expression profile in relevant cell types, and that we can estimate the parameters of the function from the data in an empirical Bayesian framework. In xTADA, we set the function to be a sigmoid function with three parameters. In VBASS, we use deep neural networks to approximate the function and learn the contribution of cell types jointly with genetic data. Using simulation, we showed that both models have accurate error rate control and better statistical power than existing methods.

We applied xTADA to a published CHD DNV data set and estimated that high-expression genes are approximately 3 times more likely to be risk genes than low-expression genes in developing heart. We identified 14 more candidate risk genes, 6 of which have additional support in independent cohorts. We applied VBASS to a published ASD DNV data set and identified 5 and 6 more candidate genes at significance level 0.05 and 0.1 respectively, 8 of them have literature support or additional genetic evidence in neurodevelopmental disorders. Moreover, we showed that gene expression profiles of GABAergic neurons and dopaminergic neurons during gestation week 9-10 are strongly associated with autism risk, indicating their potential roles in neural circuits formation.

Both methods are based on the biological hypothesis that gene expression level in relevant cell or tissue types informs the plausibility of being a disease risk gene. xTADA is optimized for a single expression profile that is informative of disease risk, such as bulk RNA sequencing data for congenital heart disease. VBASS is optimized for single cell RNA-seq data and the conditions in which multiple cell types and time points are associated with disease risk. One alternative approach to improve power based on informative non-genetic data is to calculate p-values for each gene using genetic data and then optimize FDR estimation using non-genetic data as covariates[40-42], While it is a generalizable approach, these methods require p-values to have proper distributions (uniform) under the null. In the analysis of *de novo* or ultra-rare variants, the data is usually too sparse to support a proper distribution of p-values under the null. xTADA and VBASS do not have this limitation. However, we note that VBASS can only infer the association of cell types with disease but not causality. The performance of VBASS is partially determined by how well the expression data captures true expression states of genes. In this study, we used average expression of genes in cells within a cell type inferred from single cell data and this approach has limitations in representing rare and transient cellular states. More advanced representation, like RNA velocity[43,44], together with more comprehensive measurements of cell types may improve the model.

Finally, we note the inference part of VBASS is not limited to scRNA-seq data but could be extended to other functional genomics modalities of genes, like scATAC-seq data or regulator-targets information without much modification of architecture. While the statistical part of VBASS is not limited to test the enrichment of *de novo* variants but could also be extended to inherited variants.

Methods

The probabilistic model of x-TADA and VBASS

x-TADA assumes the number of genetic variants of interest m (e.g., LGD, likely gene disruption, or Dmis, damage missense, de novo variants) and ranked expression level of a gene are drawn independently through this generative process:

$$H_0: m \sim Poisson(M), S \sim Uniform(0,1)$$

$$H_1: R \sim Gamma(\bar{\gamma}, \bar{\beta}), m \sim Poisson(R * M), S \sim Sigmoid(A, B, C)$$

Here M is the background mutation rate and S is the ranked expression level. The sigmoid function distribution is given by:

$$Sigmoid(S|A,B,C) = C + \frac{L}{1 + A * \exp{(-S + B)}}$$

where $L = (1 - C) * \frac{A}{\log(\exp(A) + \exp(A*B)) - \log{(\exp(A*B) + 1)}}$

The likelihood term is given by:

$$likelihood = \pi * GammaPoisson\left(M \middle| \bar{\gamma}, \bar{\beta}, m\right) * Sigmoid(S|A,B,C) + (1 - \pi) * Poisson(M|m)$$

There are six parameters to be estimated, $\pi, \bar{\gamma}, \bar{\beta}, A, B, C$. All of them are estimated jointly from whole gene set in an unbiased manner using MCMC via rstan package with 4 chains and 2000 iterations. The estimated parameters were used to calculate the posterior probability of association (PPA) for each gene being risk or not:

$$PPA = \frac{\pi * GammaPoisson\left(M \middle| \bar{\gamma}, \bar{\beta}, m\right) * Sigmoid(S|A,B,C)}{\pi * GammaPoisson\left(M \middle| \bar{\gamma}, \bar{\beta}, m\right) * Sigmoid(S|A,B,C) + (1 - \pi) * Poisson(M|m)}$$

VBASS assumes the number of genetic variants of interest (LGD or Dmis de novo variants) in the gene d_{gv} are drawn independently through this generative process:

$$y_g \sim Bernoulli(\pi_g)$$

$$k_{gv} = \begin{cases} \overline{k_v} \; if \; y_g = 1 \\ 1 \; otherwise \end{cases}$$

$$\theta_{gv} = \begin{cases} \overline{\theta_v} \; if \; y_g = 1 \\ 1 \; otherwise \end{cases}$$

$$\gamma_{gv} \sim \begin{cases} Gamma(k_{gv}, \theta_{gv}) \; if \; y_g = 1 \\ 1 \; otherwise \end{cases}$$

$$d_{gv} \sim \begin{cases} Poisson(\gamma_{gv} * M_{gv}) \; if \; y_g = 1 \\ Poisson(M_{gv}) \; otherwise \end{cases}$$

π_g is a gene specific prior probability of being disease risk. y_g is a binary random variable that indicates whether the gene is a risk gene or not. It is also used to generate a mixture of posterior probabilities on effect size γ_{gv}.

We use neural network f_E to infer π_g from gene expression data x_g with KL penalty of a fixed Bernoulli prior. In practice, there are 80 cell types and 2 *de novo* variant types (LGD and Dmis) for input. By default, we used a 32-dim encoding module, followed by a 2-dim sampler module for π, respectively. Each module consists of a linear layer followed by ELU activation and layer normalization layers. We apply the same reparameterization trick as conventional variational autoencoders in f_E with Bernoulli sampler[45].

The loss function is given by the evidence lower bound (ELBO),

$$ELBO = -KL[q(y|x)||p(y)] - \mathbb{E}_{q(y|x)} \log(p(d|y))$$

The KL penalty term regularized the gene-specific prior π by the hyperparameter $\bar{\pi}$, which reflects the average proportion of risk genes:

$$KL[q(y|x)||p(y)] = KL[Bernoulli(y|\pi; f_E(x))||Bernoulli(y|\bar{\pi})]$$

The expectation term quantified the log likelihood of d conditioned on y integrated on the distributions parameterized by π:

$$\mathbb{E}_{q(y|x)} \log(p(d|y)) = \int Poisson(d|\gamma * M; \overline{k_v}, \overline{\theta_v}) * Bernoulli(y|\pi; f_E(x))dy$$

$f_E, \overline{k_v}, \overline{\theta_v}$ are the parameters to learn, we use stochastic gradient decent to estimate them. The estimated parameters were used to calculate the posterior probability of association (PPA) for each gene being risk or not:

$$PPA = \frac{\pi_g * GammaPoisson(d_{gv}|\overline{k_v}, \overline{\theta_v}, M_{gv})}{\pi_g * GammaPoisson(d_{gv}|\overline{k_v}, \overline{\theta_v}, M_{gv}) + (1 - \pi_g) * Poisson(d_{gv}|M_{gv})}$$

For both x-TADA and VBASS, given PPA of all genes, we calculate Bayesian false discovery rate (FDR) by estimated false discovery proportion following the method described in He et al., 2013[12]:

$$\mathrm{FDR}_k = \frac{\sum_{i=1}^{k}(1 - \mathrm{PPA}_i)}{k}$$

Where i is the rank index of genes (start with highest PPA), and FDR_k is the estimated FDR of the gene ranked at k.

De novo variants (DNV) and gene expression data

We obtained DNV data sets from a publication on congenital heart disease (CHD)[13] of 2,645 parent-offspring trios (Table S1) and a preprint on autism spectrum disorder (ASD)[11] of 16,616 trios (Table S2). The latter is a combined data set from exome or whole genome sequencing data of the SPARK consortium[46], Simons Simplex Collection[47], Autism Sequencing Consortium[48], and MSSNG[49]. The gene expression rank was based on bulk RNA-seq data of mouse developing heart at E14.5, inspired from previous publications[6,7]. We obtained single cell RNA-seq data of human fetal midbrain and prefrontal cortex from two publications[21,22].

Annotation of de novo variants and background mutation rate calculation

We used ANNOVAR[50] and VEP[51] to annotate variants, protein-coding consequences, and predicted damaging scores for missense variants. We classified variants as LGD (likely gene disrupting, including frameshift, stop gained/lost, start lost, splice acceptor/donor), Dmis (Damage missense variants, defined by REVEL[52] score ≥ 0.5), missense, or synonymous. For each variant type, we calculated the expected number of variants based on a background mutation rate model[7,53] given the sample size. In-frame deletions/insertions (multiple of 3 nucleotides) and other splice region variants were excluded in the following analysis. Variants in olfactory receptor genes, HLA genes or MUC gene family were excluded in further analysis.

Generation of simulation datasets

We simulated two datasets to test the xTADA and VBASS respectively. For xTADA, we first estimate the parameters based on real dataset and then used the estimated hyperparameters to generate the simulated dataset based on the Bayesian mixture model. Specifically, we randomly assigned 3.7% of genes as risk gene, then we drew the covariates (gene expression rank) of risk genes from the sigmoid distribution function. The de novo damage variants were drawn from Gamma-Poisson distribution with relative risk of 20 and 12 for LoF and Dmis, respectively. For non-risk genes, we drew covariates from a uniform distribution and de novo variants from Poisson distribution. We did the simulation under different sample sizes ranging from 2,645 to 20,000. For each sample size setting, we simulated 100 datasets and fit both models on each simulated dataset independently to estimate the hyperparameters, which were used to calculate the posterior probability of association (PPA) and then a Bayesian false discovery rate (FDR) by false discovery proportion implied by it. We performed single-tail Poisson tests independently on each simulated dataset to show the baseline statistical power, where the FDR were calculated by the Benjamini-Hochberg (BH) method.

For VBASS, the simulation is based on real single cell dataset, where we created a non-linear function that maps cell-type specific expression to prior of being risk with following steps. First, we did a singular value decomposition (SVD) on the expression data of 59 known ASD risk genes (picked randomly from SFARI[29] scored 1 genes) and 86 negative control genes (picked randomly from genes with LGD variants in control cohort[14]) (Table S3). Next, we fit a logistic regression model with elastic net penalty on the eigen vectors that explain 95% of the variance. The regression model was applied to all other genes and the output probabilities were squared and scaled to have an average of 3.2%, which matches the average proportion of risk genes estimated from extTADA model. This value served as a simulated prior of being risk, from which disease risk genes were randomly sampled. The de novo damage variants were drawn from Gamma-Poisson distribution for disease risk genes while Poisson distribution for non-risk genes with same sample size and relative risk as in real ASD dataset. We performed the simulation 50 times with same simulated prior and disease risk genes, then estimated the hyperparameters and calculate the PPA and Bayesian false discovery rate (FDR) independently on each simulated dataset for both models.

Semi-supervised Training for VBASS

We trained VBASS in a semi-supervised manner with two training steps. First, we pre-trained our model using known risk genes labeled as positives and genes that harbor LGD variants in control cohort as negatives, replacing the Bernoulli KL penalty with cross-entropy loss[54]. The known risk genes (59 in total) were randomly picked from SFARI[29] (release 2021 Q4) scored 1 genes, while negative controls (86 in total) were picked from genes with LGD variants in a control cohort[14] (Table S3). During pre-training we set large learning rate to make the model converge faster. The parameters estimated from pre-training were then used as initial values in the second step, unsupervised training, which uses all genes without labels with reduced learning rate after each epoch. In practice, we used 50 epochs of semi-supervised pretraining and 60 epochs of unsupervised training. After training, we calculated PPA for all genes using the estimated parameters. For the simulation dataset, we estimated FDR on all genes to measure the statistical power. For the real dataset, we removed the known risk genes selected as positives in training when we estimate FDR to identify candidate risk genes.

Acknowledgements

We would like to thank Dr. Wendy Chung, Dr. David Knowles, Dr. Nicholas Tatonetti, Dr. Haicang Zhang, Dr. Xueya Zhou, Dr. Xiao Fan, Yige Zhao, Joseph Obiajulu, Xi Fu, and members of Shen lab for helpful discussions. This work was supported by NIH grants R01GM120609, R03HL147197, and U01HL153009, and Simons Foundation Autism Research Initiative (SIMONS606450).

Author contributions

Conceptualization, Y.S.; Methodology, G.Z. and Y.S.; Software, G.Z.; Investigation, G.Z., Y.A.C. and Y.S.; Writing – Original Draft, G.Z. and Y.S.; Writing – Review & Editing, G.Z., Y.A.C. and Y.S.; Supervision, Y.S.; Funding Acquisition, Y.S.

Declaration of interests

The authors declare no competing interests.

Data availability

All data sets (de novo variants and gene expression data) were obtained from publications and available from the corresponding publications.

Code availability

Both xTADA and VBASS are available on Github: https://github.com/ShenLab/VBASS.

Figure 1. Model architectures. A) The architecture of x-TADA. ϕ_0 and ϕ_1 are hyperpriors to be estimated: π is the prior probability of being a risk gene; $\bar{\gamma}, \bar{\beta}$ determine the prior distribution of relative risk (R); A, B, C determine the prior distribution of gene score under H_1. M is the observed damage variant number in patient cohorts. S is the functional genomics score for each gene, and in this context, it is mouse E14.5 heart expression rank percentile; m is expected number of *de novo* variants for the gene under H_0 estimated from background mutation rate. B) The architecture of VBASS. f_E is a network to inference the gene specific parameter π_g, which parameterize the distributions of y_g. This distribution will be penalized by a Bernoulli prior via KL penalty term. This model also takes predefined labels as input, where y_g is given by one-hot encoding of the labels and the Bernoulli KL penalty is replaced with a cross-entropy loss on the real label. k_{gv}, θ_{gv} are two random variables conditioned on y_g that reconstruct the parameters of Gamma-Poisson distribution for d_{gv}.

Figure 2. Performance comparison of xTADA and extTADA on simulation data. A) Precision-recall in two models, only show the part with FDR ≤ 0.2 for extTADA and xTADA, only show the part with FDR ≤ 0.01 for Poisson test. B) Comparison of recall (y-axis) for genes sets with different mutation rates (x-axis)

Figure 3. Performance of VBASS on simulation data. A) Plot of true false discovery rate (real.FDR, y axis) at different FDR cutoff (x axis) estimated by extTADA and VBASS. B) Comparison of precision recall for extTADA and VBASS, only shown for the part with FDR ≤ 0.5. C) Scatter plot of disease risk prior (π) that we assigned in simulation (y-axis) and informed by VBASS (x-axis). Genes were colored by labels and whether used in semi-supervised training, where TN and TP correspond to true negative and true positive, respectively. D) Comparison of correlation between real disease risk prior and cell type expression (y-axis) versus correlation between VBASS informed prior and cell type expression (x-axis). Each dot represents a cell type.

Figure 4. Performance comparison of xTADA and extTADA on CHD data. A). Distribution of covariates estimated by xTADA. Red, alternative hypothesis; blue, null hypothesis. B). Genes identified by xTADA and extTADA at significance level 0.1. C). FDR of genes in extTADA (y-axis) and xTADA (x-axis), genes were colored by significance in both models (red), only in xTADA (purple) or only in extTADA (green) at significance level 0.1 (FDR ≤ 0.1).

Figure 5. Performance comparison of VBASS and extTADA on ASD data. A). FDR of genes in extTADA (y-axis) or VBASS (x-axis). B). Spearman correlation between cell type expression and disease risk prior (π). The cell types from two single cell data sets were separated and ordered by correlation with π respectively.

Table 1. Estimated xTADA parameters in CHD data. Mean, posterior mean; sd, standard error; 2.5% and 97.5%, confidence interval; n_eff, effective sample number in MCMC; Rhat, convergence diagnostic in MCMC.

	mean	sd	2.50%	97.50%	n_eff	Rhat
$\boldsymbol{\pi_0}$	0.04	0.01	0.03	0.05	1845.42	1.00
$\boldsymbol{A}$	104.15	87.67	20.01	351.78	2263.73	1.00
$\boldsymbol{B}$	0.74	0.02	0.71	0.78	2136.99	1.00
$\boldsymbol{C}$	0.28	0.10	0.09	0.47	2093.73	1.00
$\boldsymbol{\bar{\gamma}_{LGD}}$	19.95	5.43	10.32	31.87	2745.30	1.00

$\bar{\gamma}_{Dmis}$	11.79	3.60	5.81	19.36	3013.96	1.00
$\bar{\beta}_{LGD}$	0.84	0.02	0.82	0.89	2193.48	1.00
$\bar{\beta}_{Dmis}$	0.90	0.07	0.83	1.07	2144.47	1.00

Table 2. Genes identified by xTADA but not extTADA. dn_LGD, de novo LGD variants; dn_Dmis, de novo Dmis variants.

Gene Symbol	dn_LGD	dn_Dmis	xTADA FDR	Expression Rank	extTADA FDR
CHD4	0	3	0.033	0.990	0.119
FRYL	2	0	0.036	0.837	0.123
GANAB	1	1	0.039	0.934	0.133
SETD5	1	1	0.043	0.949	0.138
FLT4	2	0	0.047	0.734	0.102
CAD	0	3	0.051	0.853	0.161
MINK1	0	2	0.054	0.875	0.144
ANK3	2	0	0.062	0.948	0.177
SLIT3	1	1	0.066	0.860	0.183
KMT2C	1	2	0.069	0.792	0.188
IQGAP1	0	2	0.073	0.856	0.172
TSC1	1	1	0.080	0.728	0.110
KDM5A	0	2	0.084	0.859	0.194
FBN1	0	3	0.089	0.928	0.212

Supplementary Table 1. De novo variants of 2645 CHD trios in Jin et al 2017.

Supplementary Table 2. De novo variants of 16616 ASD trios in Zhou et al 2021.

Supplementary Table 3. Labels of genes for VBASS in semi-supervised training.

Supplementary Table 4. Posterior probabilities of all genes calculated in CHD cohort by xTADA and extTADA.

Supplementary Table 5. Posterior probabilities of all genes calculated in ASD cohort by VBASS and extTADA.

Supplementary Table 6. Posterior probabilities of all genes calculated in ASD cohort by VBASS and extTADA. Removed positive training genes when calculating FDR.

Reference:

1. Rynn, L., Cragan, J. & Correa, A. Update on overall prevalence of major birth defects - Atlanta, Georgia, 1978-2005 (Reprinted from MMWR, vol 57,m pg 1-5, 2008). *Jama-Journal of the American Medical Association* **299**, 756-758 (2008).
2. O'Roak, B.J. *et al.* Exome sequencing in sporadic autism spectrum disorders identifies severe de novo mutations. *Nat Genet* **43**, 585-9 (2011).
3. Neale, B.M. *et al.* Patterns and rates of exonic de novo mutations in autism spectrum disorders. *Nature* **485**, 242-5 (2012).
4. De Rubeis, S. *et al.* Synaptic, transcriptional and chromatin genes disrupted in autism. *Nature* **515**, 209-15 (2014).
5. Sanders, S.J. *et al.* Insights into Autism Spectrum Disorder Genomic Architecture and Biology from 71 Risk Loci. *Neuron* **87**, 1215-1233 (2015).
6. Zaidi, S. *et al.* De novo mutations in histone-modifying genes in congenital heart disease. *Nature* **498**, 220-3 (2013).
7. Homsy, J. *et al.* De novo mutations in congenital heart disease with neurodevelopmental and other congenital anomalies. *Science* **350**, 1262-6 (2015).
8. Sifrim, A. *et al.* Distinct genetic architectures for syndromic and nonsyndromic congenital heart defects identified by exome sequencing. *Nat Genet* **48**, 1060-5 (2016).
9. Qi, H. *et al.* De novo variants in congenital diaphragmatic hernia identify MYRF as a new syndrome and reveal genetic overlaps with other developmental disorders. *PLoS Genet* **14**, e1007822 (2018).
10. Satterstrom, F.K. *et al.* Large-Scale Exome Sequencing Study Implicates Both Developmental and Functional Changes in the Neurobiology of Autism. *Cell* **180**, 568-584 e23 (2020).
11. Qiao, L. *et al.* Rare and de novo variants in 827 congenital diaphragmatic hernia probands implicate LONP1 as candidate risk gene. *Am J Hum Genet* **108**, 1964-1980 (2021).
12. He, X. *et al.* Integrated model of de novo and inherited genetic variants yields greater power to identify risk genes. *PLoS Genet* **9**, e1003671 (2013).
13. Jin, S.C. *et al.* Contribution of rare inherited and de novo variants in 2,871 congenital heart disease probands. *Nat Genet* **49**, 1593-1601 (2017).
14. Iossifov, I. *et al.* The contribution of de novo coding mutations to autism spectrum disorder. *Nature* **515**, 216-21 (2014).
15. Zhou, X. *et al.* Integrating <em>de novo</em> and inherited variants in over 42,607 autism cases identifies mutations in new moderate risk genes. *medRxiv*, 2021.10.08.21264256 (2021).
16. Zuk, O. *et al.* Searching for missing heritability: designing rare variant association studies. *Proc Natl Acad Sci U S A* **111**, E455-64 (2014).
17. Zhang, C. & Shen, Y. A Cell Type-Specific Expression Signature Predicts Haploinsufficient Autism-Susceptibility Genes. *Hum Mutat* **38**, 204-215 (2017).
18. Chen, S. *et al.* Dissecting Autism Genetic Risk Using Single-cell RNA-seq Data. *bioRxiv*, 2020.06.15.153031 (2020).
19. Rozenblatt-Rosen, O., Stubbington, M.J.T., Regev, A. & Teichmann, S.A. The Human Cell Atlas: from vision to reality. *Nature* **550**, 451-453 (2017).

20. Tabula Muris, C. *et al.* Single-cell transcriptomics of 20 mouse organs creates a Tabula Muris. *Nature* **562**, 367-372 (2018).

21. La Manno, G. *et al.* Molecular Diversity of Midbrain Development in Mouse, Human, and Stem Cells. *Cell* **167**, 566-580 e19 (2016).

22. Zhong, S. *et al.* A single-cell RNA-seq survey of the developmental landscape of the human prefrontal cortex. *Nature* **555**, 524-528 (2018).

23. Cao, J. *et al.* A human cell atlas of fetal gene expression. *Science* **370**(2020).

24. He, P. *et al.* The changing mouse embryo transcriptome at whole tissue and single-cell resolution. *Nature* **583**, 760-767 (2020).

25. Nguyen, H.T. *et al.* Integrated Bayesian analysis of rare exonic variants to identify risk genes for schizophrenia and neurodevelopmental disorders. *Genome Med* **9**, 114 (2017).

26. Hinton, R.B. *et al.* Cardiovascular manifestations of tuberous sclerosis complex and summary of the revised diagnostic criteria and surveillance and management recommendations from the International Tuberous Sclerosis Consensus Group. *J Am Heart Assoc* **3**, e001493 (2014).

27. Kaplanis, J. *et al.* Evidence for 28 genetic disorders discovered by combining healthcare and research data. *Nature* **586**, 757-762 (2020).

28. Willsey, A.J. *et al.* Coexpression networks implicate human midfetal deep cortical projection neurons in the pathogenesis of autism. *Cell* **155**, 997-1007 (2013).

29. Abrahams, B.S. *et al.* SFARI Gene 2.0: a community-driven knowledgebase for the autism spectrum disorders (ASDs). *Mol Autism* **4**, 36 (2013).

30. Reiff, R.E. *et al.* METTL23, a transcriptional partner of GABPA, is essential for human cognition. *Hum Mol Genet* **23**, 3456-66 (2014).

31. Bernkopf, M. *et al.* Disruption of the methyltransferase-like 23 gene METTL23 causes mild autosomal recessive intellectual disability. *Hum Mol Genet* **23**, 4015-23 (2014).

32. Crider, A., Ahmed, A.O. & Pillai, A. Altered Expression of Endoplasmic Reticulum Stress-Related Genes in the Middle Frontal Cortex of Subjects with Autism Spectrum Disorder. *Mol Neuropsychiatry* **3**, 85-91 (2017).

33. Takahashi, M. *et al.* Hyperactive and impulsive behaviors of LMTK1 knockout mice. *Sci Rep* **10**, 15461 (2020).

34. Inoue, T. *et al.* LMTK3 deficiency causes pronounced locomotor hyperactivity and impairs endocytic trafficking. *J Neurosci* **34**, 5927-37 (2014).

35. Coghlan, S. *et al.* GABA system dysfunction in autism and related disorders: from synapse to symptoms. *Neurosci Biobehav Rev* **36**, 2044-55 (2012).

36. Rojas, D.C., Singel, D., Steinmetz, S., Hepburn, S. & Brown, M.S. Decreased left perisylvian GABA concentration in children with autism and unaffected siblings. *Neuroimage* **86**, 28-34 (2014).

37. Puts, N.A.J. *et al.* Reduced GABA and altered somatosensory function in children with autism spectrum disorder. *Autism Res* **10**, 608-619 (2017).

38. Chao, O.Y. *et al.* Altered dopaminergic pathways and therapeutic effects of intranasal dopamine in two distinct mouse models of autism. *Mol Brain* **13**, 111 (2020).

39. Kosillo, P. & Bateup, H.S. Dopaminergic Dysregulation in Syndromic Autism Spectrum Disorders: Insights From Genetic Mouse Models. *Front Neural Circuits* **15**, 700968 (2021).

40. Ignatiadis, N., Klaus, B., Zaugg, J.B. & Huber, W. Data-driven hypothesis weighting increases detection power in genome-scale multiple testing. *Nat Methods* (2016).
41. Zhang, M.J., Xia, F. & Zou, J. Fast and covariate-adaptive method amplifies detection power in large-scale multiple hypothesis testing. *Nat Commun* **10**, 3433 (2019).
42. Yurko, R., G'Sell, M., Roeder, K. & Devlin, B. A selective inference approach for false discovery rate control using multiomics covariates yields insights into disease risk. *Proc Natl Acad Sci U S A* **117**, 15028-15035 (2020).
43. La Manno, G. *et al.* RNA velocity of single cells. *Nature* **560**, 494-498 (2018).
44. Bergen, V., Lange, M., Peidli, S., Wolf, F.A. & Theis, F.J. Generalizing RNA velocity to transient cell states through dynamical modeling. *Nature Biotechnology* **38**(2020).
45. Kingma, D.P. & Welling, M. Auto-Encoding Variational Bayes. arXiv:1312.6114 (2013).
46. pfeliciano@simonsfoundation.org, S.C.E.a. & Consortium, S. SPARK: A US Cohort of 50,000 Families to Accelerate Autism Research. *Neuron* **97**, 488-493 (2018).
47. Coe, B.P. *et al.* Neurodevelopmental disease genes implicated by de novo mutation and copy number variation morbidity. *Nat Genet* **51**, 106-116 (2019).
48. Buxbaum, J.D. *et al.* The autism sequencing consortium: large-scale, high-throughput sequencing in autism spectrum disorders. *Neuron* **76**, 1052-6 (2012).
49. RK, C.Y. *et al.* Whole genome sequencing resource identifies 18 new candidate genes for autism spectrum disorder. *Nat Neurosci* **20**, 602-611 (2017).
50. Wang, K., Li, M. & Hakonarson, H. ANNOVAR: functional annotation of genetic variants from high-throughput sequencing data. *Nucleic Acids Res* **38**, e164 (2010).
51. McLaren, W. *et al.* The Ensembl Variant Effect Predictor. *Genome Biol* **17**, 122 (2016).
52. Ioannidis, N.M. *et al.* REVEL: An Ensemble Method for Predicting the Pathogenicity of Rare Missense Variants. *Am J Hum Genet* **99**, 877-885 (2016).
53. Samocha, K.E. *et al.* A framework for the interpretation of de novo mutation in human disease. *Nat Genet* **46**, 944-50 (2014).
54. Kingma, D.P., Rezende, D.J., Mohamed, S. & Welling, M. Semi-Supervised Learning with Deep Generative Models. arXiv:1406.5298 (2014).

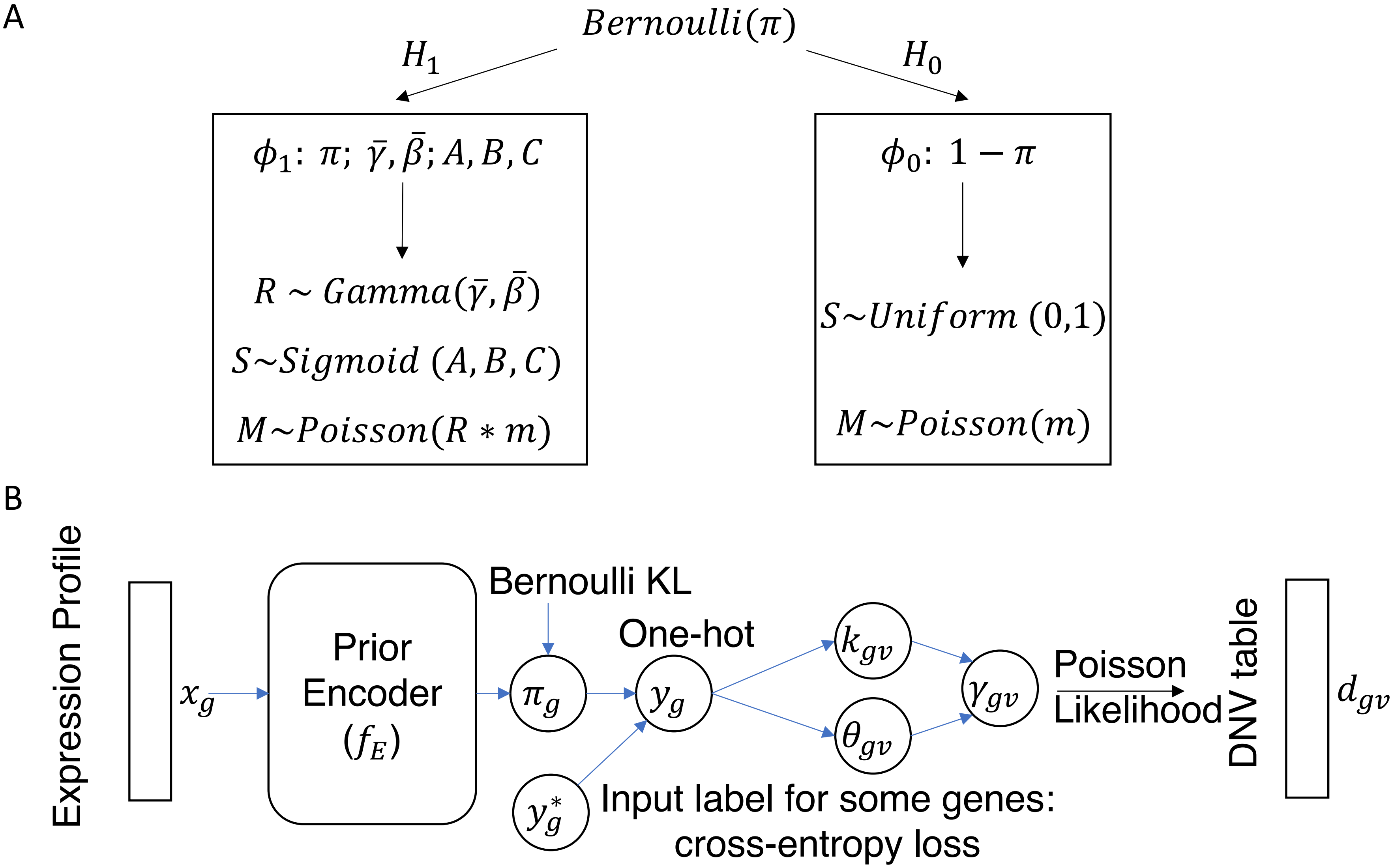
A
$Bernoulli(\pi)$
H_1
H_0
ϕ_1: π; $\bar{\gamma}, \bar{\beta}$; A, B, C
$R \sim Gamma(\bar{\gamma}, \bar{\beta})$
$S \sim Sigmoid\ (A, B, C)$
$M \sim Poisson(R * m)$
ϕ_0: $1 - \pi$
$S \sim Uniform\ (0,1)$
$M \sim Poisson(m)$
B
Expression Profile
x_g
Prior Encoder (f_E)
Bernoulli KL
π_g
One-hot
y_g
y_g^*
k_{gv}
θ_{gv}
γ_{gv}
Poisson Likelihood
DNV table
d_{gv}
Input label for some genes: cross-entropy loss

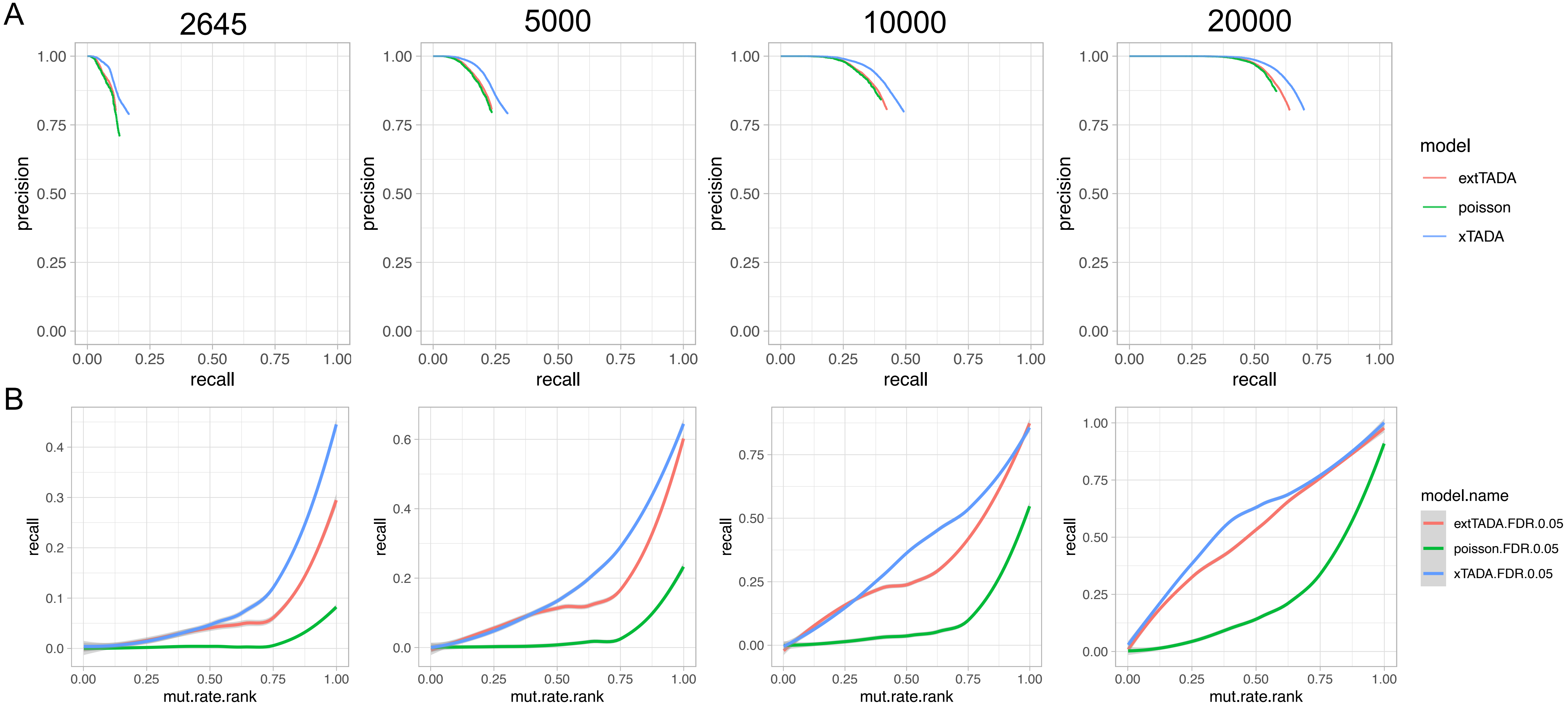
A
2645
5000
10000
20000
precision
1.00
0.75
0.50
0.25
0.00
recall
0.00
0.25
0.50
0.75
1.00
model
extTADA
poisson
xTADA
B
recall
mut.rate.rank
0.0
0.1
0.2
0.3
0.4
0.6
model.name
extTADA.FDR.0.05
poisson.FDR.0.05
xTADA.FDR.0.05

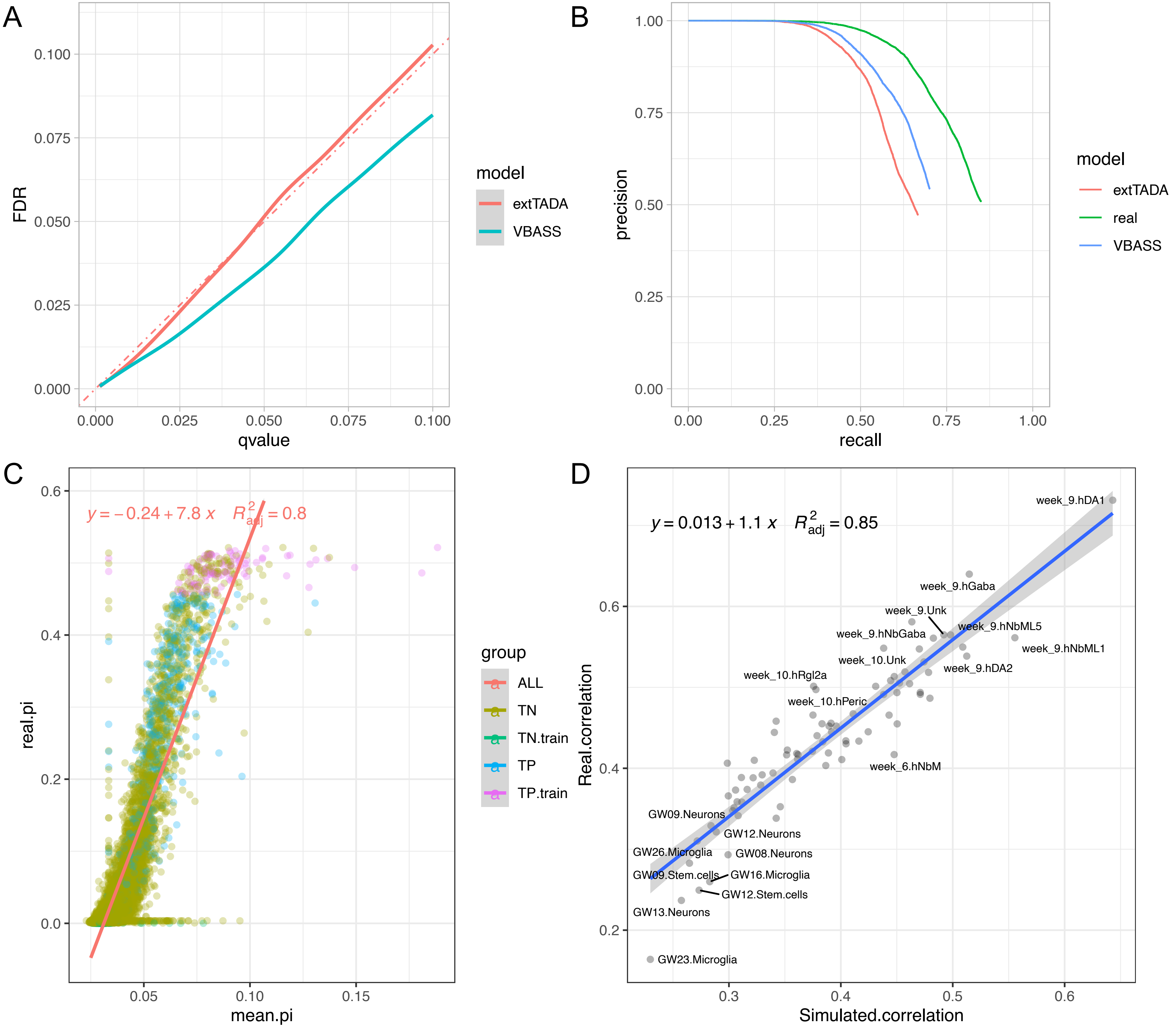
A
0.100
0.075
0.050
0.025
0.000
FDR
0.000
0.025
0.050
0.075
0.100
qvalue
model
extTADA
VBASS
B
1.00
0.75
0.50
0.25
0.00
precision
0.00
0.25
0.50
0.75
1.00
recall
model
extTADA
real
VBASS
C
$y = -0.24 + 7.8\ x \quad R^2_{adj} = 0.8$
0.6
0.4
0.2
0.0
real.pi
0.05
0.10
0.15
mean.pi
group
ALL
TN
TN.train
TP
TP.train
D
$y = 0.013 + 1.1\ x \quad R^2_{adj} = 0.85$
week_9.hDA1
week_9.hGaba
week_9.Unk
week_9.hNbML5
week_9.hNbGaba
week_9.hNbML1
week_10.Unk
week_9.hDA2
week_10.hRgl2a
week_10.hPeric
week_6.hNbM
GW09.Neurons
GW12.Neurons
GW26.Microglia
GW08.Neurons
GW09.Stem.cells
GW16.Microglia
GW12.Stem.cells
GW13.Neurons
GW23.Microglia
0.6
0.4
0.2
Real.correlation
0.3
0.4
0.5
0.6
Simulated.correlation

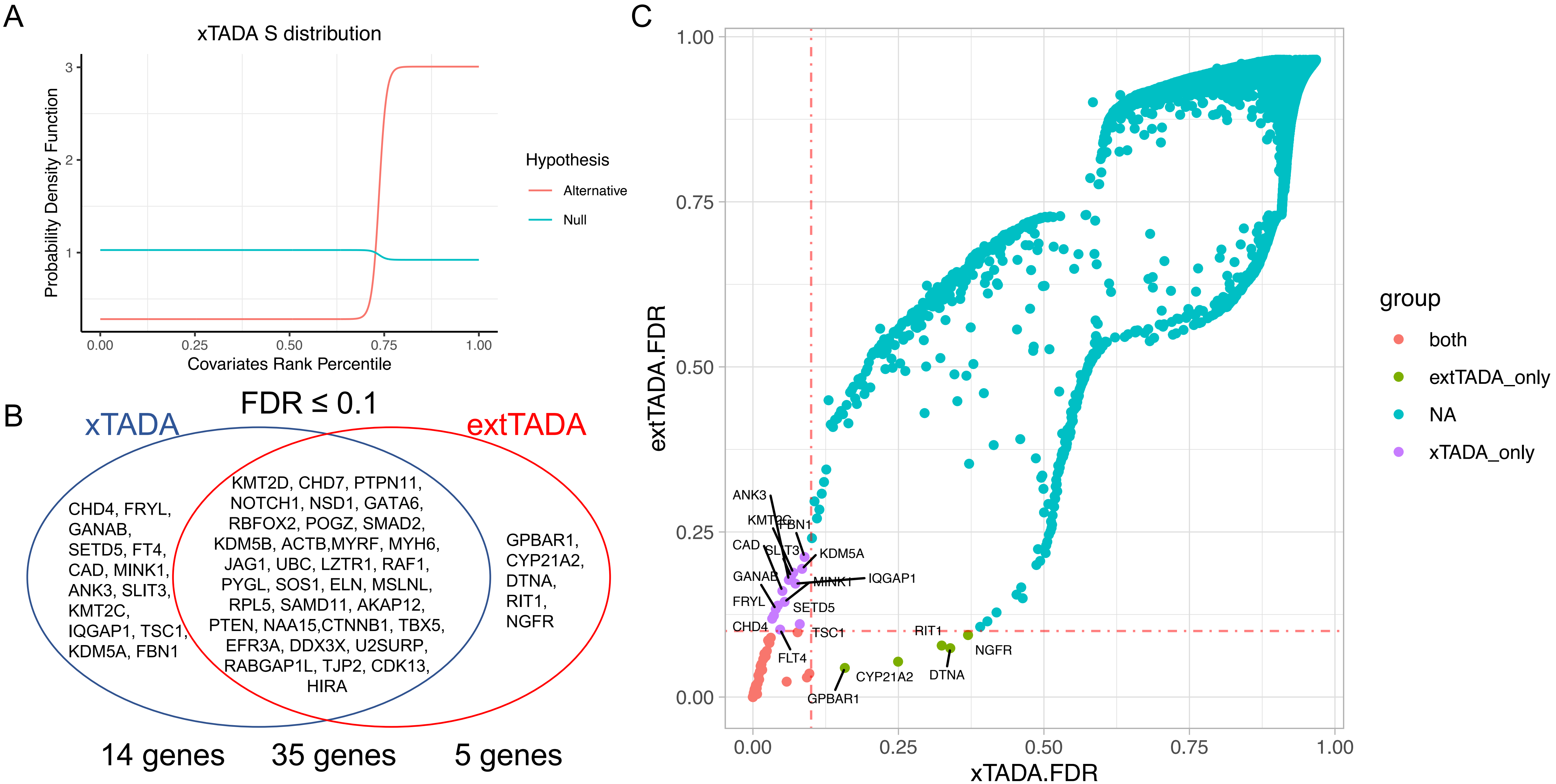
A
xTADA S distribution
Probability Density Function
3
2
1
0.00
0.25
0.50
0.75
1.00
Covariates Rank Percentile
Hypothesis
Alternative
Null
B
FDR ≤ 0.1
xTADA
extTADA
CHD4, FRYL, GANAB, SETD5, FT4, CAD, MINK1, ANK3, SLIT3, KMT2C, IQGAP1, TSC1, KDM5A, FBN1
KMT2D, CHD7, PTPN11, NOTCH1, NSD1, GATA6, RBFOX2, POGZ, SMAD2, KDM5B, ACTB,MYRF, MYH6, JAG1, UBC, LZTR1, RAF1, PYGL, SOS1, ELN, MSLNL, RPL5, SAMD11, AKAP12, PTEN, NAA15,CTNNB1, TBX5, EFR3A, DDX3X, U2SURP, RABGAP1L, TJP2, CDK13, HIRA
GPBAR1, CYP21A2, DTNA, RIT1, NGFR
14 genes
35 genes
5 genes
C
1.00
0.75
0.50
0.25
0.00
extTADA.FDR
0.00
0.25
0.50
0.75
1.00
xTADA.FDR
ANK3
KMT2C
FBN1
CAD
SLIT3
KDM5A
GANAB
MINK1
IQGAP1
FRYL
SETD5
CHD4
TSC1
FLT4
RIT1
NGFR
CYP21A2
DTNA
GPBAR1
group
both
extTADA_only
NA
xTADA_only

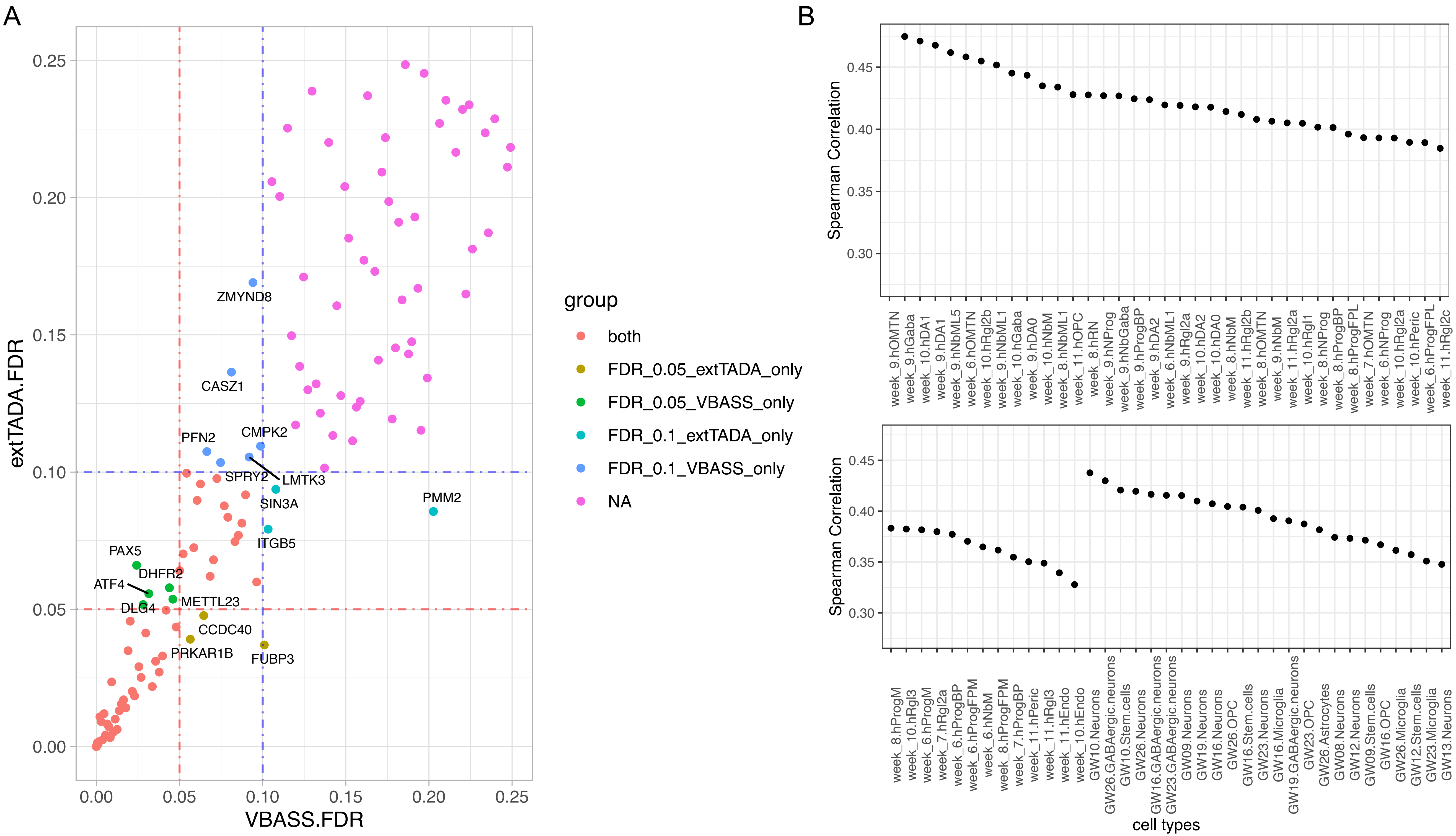
A
0.25
0.20
0.15
0.10
0.05
0.00
extTADA.FDR
0.00
0.05
0.10
0.15
0.20
0.25
VBASS.FDR
ZMYND8
CASZ1
PFN2
CMPK2
SPRY2
LMTK3
SIN3A
PMM2
ITGB5
PAX5
DHFR2
ATF4
DLG4
METTL23
CCDC40
PRKAR1B
FUBP3
group
both
FDR_0.05_extTADA_only
FDR_0.05_VBASS_only
FDR_0.1_extTADA_only
FDR_0.1_VBASS_only
NA
B
Spearman Correlation
0.45
0.40
0.35
0.30
week_9.hOMTN
week_9.hGaba
week_10.hDA1
week_9.hDA1
week_9.hNbML5
week_6.hOMTN
week_10.hRgl2b
week_9.hNbML1
week_10.hGaba
week_9.hDA0
week_10.hNbM
week_8.hNbML1
week_11.hOPC
week_8.hRN
week_9.hNProg
week_9.hNbGaba
week_9.hProgBP
week_9.hDA2
week_6.hNbML1
week_9.hRgl2a
week_10.hDA2
week_10.hDA0
week_8.hNbM
week_11.hRgl2b
week_8.hOMTN
week_9.hNbM
week_11.hRgl2a
week_10.hRgl1
week_8.hNProg
week_8.hProgBP
week_8.hProgFPL
week_7.hOMTN
week_6.hNProg
week_10.hRgl2a
week_10.hPeric
week_6.hProgFPL
week_11.hRgl2c
Spearman Correlation
0.45
0.40
0.35
0.30
week_8.hProgM
week_10.hRgl3
week_6.hProgM
week_7.hRgl2a
week_6.hProgBP
week_6.hProgFPM
week_6.hNbM
week_8.hProgFPM
week_7.hProgBP
week_11.hPeric
week_11.hRgl3
week_11.hEndo
week_10.hEndo
GW10.Neurons
GW26.GABAergic.neurons
GW10.Stem.cells
GW26.Neurons
GW16.GABAergic.neurons
GW23.GABAergic.neurons
GW09.Neurons
GW19.Neurons
GW16.Neurons
GW26.OPC
GW16.Stem.cells
GW23.Neurons
GW16.Microglia
GW19.GABAergic.neurons
GW23.OPC
GW26.Astrocytes
GW08.Neurons
GW12.Neurons
GW09.Stem.cells
GW16.OPC
GW26.Microglia
GW12.Stem.cells
GW23.Microglia
GW13.Neurons
cell types